AIAA JOURNAL
Vol. 33, No. 11, November 1995

Shape Design for Thin-Walled Beam Cross Sections Using Rational *B* Splines

Uwe Schramm* and Walter D. Pilkey†
University of Virginia, Charlottesville, Virginia 22903-2442
and
Richard I. DeVries‡ and Mark P. Zebrowski‡
Ford Motor Company, Dearborn, Michigan 48121-2053

Shape optimization of thin-walled beams is discussed. The cross-sectional shape of the beam is described by nonuniform rational *B*-spline curves. The optimization problem is defined in terms of cross-sectional properties and stresses. Design variables are the control parameters of the rational *B*-spline curves and the wall thickness of the beam. Cross-sectional properties and stresses are obtained from the elasticity solution for the beam. Consideration of torsion and pure shear requires the solution of Laplace equations which is accomplished using finite elements. A design sensitivity analysis is given for the cross-sectional properties and stresses. A sample problem is presented to illustrate the formulations.

Introduction

In the design of metal structures, thin-walled beams are important elements. Optimization of these elements can lead to significant cost reductions. This study was motivated by applications of thin-walled beams in automobile design.[1] However, its results are applicable to other branches of metal structural design, such as aerospace and ocean engineering. Figure 1 shows an example of a beam manufactured from two thin-walled parts which are welded together. Such beams are members of a complex structure. The structure is analyzed using finite beam elements, and the beam cross-sectional properties and stresses can be found from the elasticity solution of the beam. Optimization of the structure is performed to obtain certain strength characteristics and a structural mass that is as low as possible. The structural optimization problem may be expressed as follows.

Objective function:

$$W(\boldsymbol{p}) \Rightarrow \min \tag{1a}$$

Inequality constraints:

$$\boldsymbol{g}(\boldsymbol{p}) \leq \boldsymbol{0} \tag{1b}$$

Equality constraints:

$$\boldsymbol{h}(\boldsymbol{p}) = \boldsymbol{0} \tag{1c}$$

Side constraints:

$$\boldsymbol{p}^l \leq \boldsymbol{p} \leq \boldsymbol{p}^u \tag{1d}$$

The objective function W may be the beam cross-sectional area or any other cross-sectional property. As constraints $g_i \in \boldsymbol{g}$, cross-sectional properties or stresses may be applied. Here, the shape of the beam cross section will be modified to obtain an optimal structural design. Hence, the design variables $p_j \in \boldsymbol{p}$ are values describing the shape of the cross section. The equality constraints describe dependencies of design variables. The side constraints, which are inequalities, on the design variables are treated separately. Either the objective function or constraints may be the result of further computation based on the cross-sectional properties, such as responses computed from a finite element analysis to which beam cross section properties were provided as input.

Analysis of the design process indicates that major contributions to the design are created by computer-aided design (CAD) tools. The final design is analyzed using numerical procedures such as finite elements. Currently, separate preprocessors for the definition of the numerical models are used. Design optimization and design sensitivity analysis is then based on the numerical model. It appears that in practice different geometry definitions are used for design, analysis, and optimization. But the internal definition of the design geometry in CAD systems is based on geometric elements which are also useful in numerical analysis and design. In particular, nonuniform rational *B* splines (NURBs), a special type of *B* splines, are widely used for this purpose.[2] They have been implemented recently in CAD systems and product data interfaces of several automobile manufacturers.[3] Here, the approach to the connection of CAD with analysis and optimization is to use the geometric definition of CAD also in the numerical models for analysis and optimization. Bezier-and *B*-spline curves and surfaces have been successfully applied in shape optimal design for the numerical description of the structural shape.[4–8] The subject of this presentation is the application of the description of the cross-sectional shape of thin-walled beams using NURB curves. The cross-sectional shape will be modified changing the shape of the defining NURB curves. Hence, the control parameters of the NURB curves are the design variables. Additionally, the wall thickness will serve as a design variable.

This presentation will be restricted to shape optimization of the cross section of cantilever beams with the load applied on the free end only. If the beam is included in a more complex frame structure, the changes of the loads due to changes in the cross-sectional shape of structural members may have to be taken into consideration.

Analysis of Thin-Walled Beams

The analysis of the thin-walled beam will be accomplished using the elasticity solution for the beam.[9,10] In this section the stresses and cross-sectional properties of the beam will be given. Both can be used as objectives and constraints in the optimization problem of Eq. (1).

Figure 1 shows the problem to be solved. The coordinate system is chosen with its origin at the centroid of the cross section of the clamped end; x is the axial coordinate and y, z are the cross-sectional coordinates. The cross-sectional axes may be of arbitrary orientation. The loads are the torsional moment M_x and the components

Received July 19, 1994; presented as Paper 94-4392 at the AIAA/USAF/NASA/ISSMO 5th Symposium on Multidisciplinary Analysis and Optimization, Panama City Beach, FL, Sept. 7–9, 1994; revision received Jan. 11, 1995; accepted for publication Jan. 11, 1995. Copyright © 1994 by the American Institute of Aeronautics and Astronautics, Inc. All rights reserved.

*Senior Scientist, Department of Mechanical, Aerospace, and Nuclear Engineering, Thornton Hall.
†Frederick T. Morse Professor, Department of Mechanical, Aerospace, and Nuclear Engineering, Thornton Hall.
‡Advanced Vehicle System Engineering.

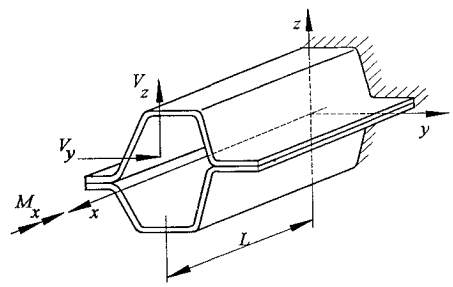

Fig. 1 Thin-walled beam.

V_y and V_z of the shear force $\boldsymbol{V}$ that may be applied to a point of the cross section such that they cause no additional torsion. No body forces are applied. The material of the beam is linearly elastic, homogeneous, and isotropic, with Young's modulus E, Poisson's ratio ν, and shear modulus $G = E/2(1+\nu)$. The stresses σ_{yy}, σ_{zz} and τ_{yz} are zero.

Stresses

According to Ref. 9 the shear stresses in beams can be determined from the elasticity equations. The normal stresses σ_{xx} due to bending follow from the kinematic assumptions of the Euler–Bernoulli theory. They are

$$\sigma_{xx} = -(L-x)\boldsymbol{S}^{-1}\begin{bmatrix} y \\ z \end{bmatrix} \tag{2}$$

where the matrix $\boldsymbol{S}$ contains the moments of inertia I_{qr}, $\boldsymbol{S} = \{I_{qr}\} = \{\int_A qr\ \mathrm{d}A\}$, $q, r = y, z$. The shear stresses $\tau = \{\tau_{xy}, \tau_{xz}\}$ can be obtained from the compatibility equations,[9] leading to

$$\tau = \{(\nabla\psi_x - \boldsymbol{g}_x)\phi_x' + (\nabla\psi_y - \boldsymbol{g}_y)V_y + (\nabla\psi_z - \boldsymbol{g}_z)V_z\} \tag{3}$$

where ψ_q, $q = x, y, z$, often called warping functions, are functions of y and z, and ϕ_x' is the rate of angle of twist of the centroidal beam axis. The vectors $\boldsymbol{g}_q$ are

$$\boldsymbol{g}_x = \begin{bmatrix} z \\ -y \end{bmatrix} \tag{4}$$

$$\boldsymbol{g}_y = \frac{1}{E\det\boldsymbol{S}}\begin{bmatrix} (1+\nu)y^2 - \nu z^2 & 0 \\ 0 & (1+\nu)z^2 - \nu y^2 \end{bmatrix}^T \begin{bmatrix} I_{zz} \\ -I_{yz} \end{bmatrix} \tag{5}$$

$$\boldsymbol{g}_z = \frac{1}{E\det\boldsymbol{S}}\begin{bmatrix} (1+\nu)y^2 - \nu z^2 & 0 \\ 0 & (1+\nu)z^2 - \nu y^2 \end{bmatrix}^T \begin{bmatrix} -I_{yz} \\ I_{yy} \end{bmatrix} \tag{6}$$

Introduction of the stresses into the equilibrium relationships yields three independent Laplace equations,

$$-\nabla^2\psi_q = 0, \qquad q = x, y, z \tag{7}$$

The corresponding boundary conditions

$$\frac{\partial\psi_q}{\partial\hat{\boldsymbol{n}}} = \boldsymbol{g}_q^T\hat{\boldsymbol{n}}, \qquad q = x, y, z \tag{8}$$

follow from the condition that the boundary of the cross section is traction free. The vector $\hat{\boldsymbol{n}}$ is the outward directed normal on the boundary.

Cross-Sectional Properties

Beam cross-sectional properties can be separated into those that depend on warping functions and those that do not. The latter are the cross-sectional area A, the moments of inertia I_{yy}, I_{yz}, and I_{zz} and the centroid of the cross section $\boldsymbol{c} = \{c_y, c_z\}$. The other properties are the torsional constant I_t, the shear deformation coefficients α_{yy}, α_{yz}, and α_{zz} and the shear center $\boldsymbol{s} = \{s_y, s_z\}$. These quantities can be found from the strain energy U_τ due to torsion and pure shear. The strain energy U_τ can be written as

$$U_\tau = \frac{1}{2G}\int_L\int_A \left(\tau_{xy}^2 + \tau_{xz}^2\right)\mathrm{d}A\ \mathrm{d}x \tag{9}$$

Introduction of τ_{xy} and τ_{xz} of Eq. (3) leads to

$$U_\tau = \frac{1}{2G}\int_L G^2\left[a_{xx}\phi_x'^2 + a_{yy}V_y^2 + a_{zz}V_z^2 + 2a_{xy}\phi_x'V_y + 2a_{xz}\phi_x'V_z + 2a_{yz}V_yV_z\right]\mathrm{d}x \tag{10}$$

with the constants

$$a_{qr} = \int_A (\nabla\psi_q)^T\nabla\psi_r\ \mathrm{d}A - \int_A (\nabla\psi_q)^T\boldsymbol{g}_r\ \mathrm{d}A - \int_A (\nabla\psi_r)^T\boldsymbol{g}_q\ \mathrm{d}A + \int_A^T \boldsymbol{g}_r\boldsymbol{g}_q\ \mathrm{d}A, \qquad q, r = x, y, z \tag{11}$$

From this, the torsional constant appears as $I_t = a_{xx}$, the shear deformation coefficients are $\alpha_{qr} = G^2Aa_{qr}$, $q, r = y, z$, and the coefficients that account for the coupling of pure shear and torsion are Ga_{xz} and Ga_{xy}. Consideration of the equilibrium of moments leads to the shear center $\boldsymbol{s}$ and to the rate of angle of twist ϕ_x'.

Finite Element Solution

Because of its applicability to any cross-sectional shape, a finite element method is preferred here to solve Eqs. (7). Using Galerkin's method, the elementwise approximation $\psi_q^e = \boldsymbol{N}\boldsymbol{d}_q^e$, $q = x, y, z$, leads to

$$\boldsymbol{K}^e\boldsymbol{d}_q^e = \boldsymbol{f}_q^e \tag{12}$$

with

$$\boldsymbol{K}^e = \int_{-1}^{+1}\int_{-1}^{+1} \boldsymbol{B}^T\boldsymbol{B}\det\boldsymbol{J}\ \mathrm{d}\xi\ \mathrm{d}\eta \tag{13}$$

$$\boldsymbol{f}_q^e = \boldsymbol{f}_{q1}^e + \boldsymbol{f}_{q2}^e = \int_{-1}^{+1}\int_{-1}^{+1} \left\{\boldsymbol{B}^T\boldsymbol{g}_q + \boldsymbol{N}^T\nabla^T\boldsymbol{g}_q\right\}\det\boldsymbol{J}\ \mathrm{d}\xi\ \mathrm{d}\eta \tag{14}$$

The matrix $\boldsymbol{B}$ is defined as $\boldsymbol{B} = \nabla\boldsymbol{N}$. The scalar $\det\boldsymbol{J}$ is the determinant of the Jacobian $\boldsymbol{J}$. Compatibility of the nodal values of $\boldsymbol{d}_q^e$ leads to three systems of linear equations,

$$\boldsymbol{K}\boldsymbol{d}_q = \boldsymbol{f}_q \tag{15}$$

which can be solved simultaneously since they all have the same coefficient matrix. For each element in derivatives $\nabla\psi_q$ may be calculated from

$$\nabla\psi_q = \boldsymbol{B}\boldsymbol{d}_q^e \tag{16}$$

Then, stresses and cross-sectional properties follow. To get the nodal stresses, the nodal derivatives $\nabla\psi_q$ are extrapolated from the Gauss points using the shape functions $\boldsymbol{N}$ and then averaged at the nodes. From Eq. (15), the coefficients a_{qr}, $q, r = x, y, z$ appear as

$$a_{qr} = a_{qr1} - a_{qr2} - a_{rq2} + a_{qr3} \tag{17}$$

with

$$a_{qr1} = \boldsymbol{d}_q^T\boldsymbol{K}\boldsymbol{d}_r, \qquad a_{qr2} = \boldsymbol{d}_q^T\boldsymbol{f}_{r1}, \qquad a_{qr3} = \int_A \boldsymbol{g}_r^T\boldsymbol{g}_q\ \mathrm{d}A \tag{18}$$

The area integrals that are necessary to obtain some cross-sectional properties are calculated from the element integration scheme.

Description of the Structural Shape

The shape of the thin-walled cross section is determined by NURB curves and the wall thickness t (Fig. 2). Additional information is the number of finite elements along the length of the spline, μ_γ, and through the thickness, μ_n.

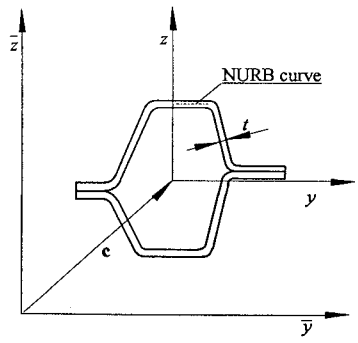

Fig. 2 Beam cross section.

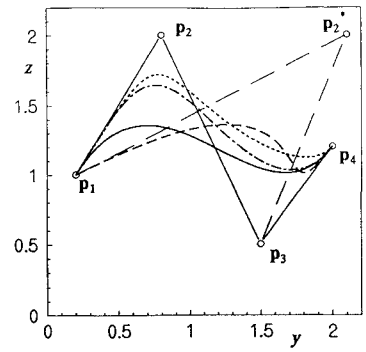

Fig. 3 NURB curves: solid line, $\chi = m = 4, w_j = 1$; dashed line, p_2 moved to p_2^*; dotted line, $w_2 = 4$; dash-dot line, p_2 used twice; thinner lines, defining polygons.

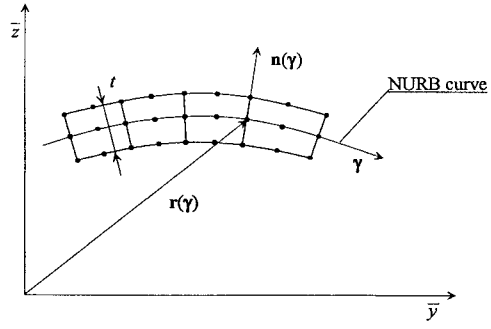

Fig. 4 Finite element mapping, $\zeta_n = 1$.

Nonuniform Rational *B* Splines

The position vector $\boldsymbol{r}(\gamma) = \{r_y, r_z\}$ of a point of a rational B-spline curve of the order χ is defined as a linear combination of m vertices $\boldsymbol{p}_j = \{p_{jy}, p_{jz}\}$

$$\boldsymbol{r}(\gamma) = \sum_{j=1}^{m} \boldsymbol{p}_j \hat{b}_{j\chi}(\gamma) \tag{19}$$

using

$$\hat{b}_{j\chi}(\gamma) = [w_j b_{j\chi}(\gamma)] \Big/ \sum_{q=1}^{m} w_q b_{q\chi}(\gamma) \tag{20}$$

with the B-spline basis $b_{j\chi}(\gamma)$ obtained from a recursion formula.[2,8,11] The values w_j are weights assigned to the vertices such that a vertex has a fourth coordinate in addition to its three physical coordinates. The dimensionless quantity γ is the parameter of the curve. It can take all values between zero and $\bar{\gamma} = m - \chi + 1$. The vertices $\boldsymbol{p}_j$ form the defining polygon. In the case where all weights w_j are equal to one, rational B-spline curves are identical to nonrational B splines. NURB curves have the following characteristics. 1) The curve lies in a convex hull of the vertices. 2) The curve is invariant under an affine transformation. 3) The tangents of the initial and final points are defined by the first and the last edge, respectively, of the defining polygon. 4) The position vector $\boldsymbol{r}(\gamma)$ and its derivatives up to order $\chi - 2$ are all continuous over the entire curve. The NURB curve can be altered by changing the number and/or position of the vertices of the defining polygon, by changing the weights w_j, by changing the order χ, and by the use of repeated vertices (Fig. 3).

For the definition of the finite element mesh the derivatives of the curves with respect to the parameter γ are necessary. Differentiation of Eq. (19) leads to

$$\boldsymbol{r}^{(n)}(\gamma) = \frac{\partial^n \boldsymbol{r}(\gamma)}{\partial \gamma^n} = \sum_{j=1}^{m} \boldsymbol{p}_j \hat{b}_{j\chi}^{(n)}(\gamma) \tag{21}$$

with

$$\hat{b}_{j\chi}^{(n)}(\gamma) = \frac{\partial^n \hat{b}_{j\chi}(\gamma)}{\partial \gamma^n}$$

$$= \left(1 \Big/ \sum_{q=1}^{m} w_q b_{q\chi}\right)\left\{ w_j b_{j\chi}^{(n)} - \sum_{l=0}^{n-1} \left[\binom{n}{l} \hat{b}_{j\chi}^{(l)} \sum_{q=1}^{m} b_{q\chi}^{(n-l)} \right] \right\} \tag{22}$$

It will be agreed that $\hat{b}_{j\chi}^{(0)}$ stands for $\hat{b}_{j\chi}$. Again, the derivatives of the B-spline basis $\hat{b}_{j\chi}^{(n)}$ are obtained from a recursion formula. From the derivative $\boldsymbol{r}'(\gamma) = \boldsymbol{r}^{(1)}(\gamma)$ of Eq. (21), the normal unit vector $\boldsymbol{n}(\gamma)$ on the curve at the point $\boldsymbol{r}(\gamma)$ is obtained. If the cross section is defined in an arbitrary coordinate system $\bar{y}, \bar{z}$, the transformation

$$\boldsymbol{x} = \{y, z\} = \boldsymbol{r} - \boldsymbol{c} \tag{23}$$

must be applied, where $\boldsymbol{c} = \{c_y, c_z\}$ is the centroid of the cross section defined in the $\bar{y}, \bar{z}$ system (Fig. 2).

Finite Element Mapping

Based on the line element formulation of Ref. 12, special finite elements were developed in an earlier investigation for the analysis and optimization of thin-walled structures using NURB curves.[13] For those finite element models only one element layer through the wall thickness was used to model the cross section. This methodology is very convenient if cross-sectional properties are used as constraints, but if stresses are required, these models are not sufficient.

Here, biquadratic Lagrange type shape functions, which lead to a nine node element with one degree of freedom per node, will be used. The element mapping is isoparametric. The elements will be mapped such that the NURB curve $\boldsymbol{r}(\gamma_k)$ defines the centerline of the wall (Fig. 4). Then, the nodal coordinates of the element $\zeta_\gamma, \zeta_n, \zeta_\gamma \in \langle 1, \mu_\gamma \rangle, \zeta_n \in \langle 1, \mu_n \rangle$ are given by

$$\boldsymbol{x}^e_{3(k-1)+l} = \boldsymbol{r}(\gamma_k) + \boldsymbol{n}(\gamma_k)[(2\zeta_n - \mu_n + l - 3)/2\mu_n]t - \boldsymbol{c} \tag{24}$$

with

$$\gamma_k = [(2\zeta_\gamma + k - 3)/2\mu_\gamma]\gamma_{\max} \qquad k, l = 1, 2, 3 \tag{25}$$

More elements are concentrated in those portions of the curve with large curvature. This is because the parameter γ, which defines the finite element mesh, is not evenly distributed over the curve. If the curvature $\kappa(\gamma_k)$ is larger than $2/t$, i.e.,

$$\kappa(\gamma_k) = \frac{|\boldsymbol{n}^T(\gamma_k)\boldsymbol{r}''(\gamma_k)|}{|\boldsymbol{r}'(\gamma_k)|^3} > \frac{2}{t} \tag{26}$$

Eq. (24) cannot be used to define the nodal coordinates of the finite element mesh. In this case the domain will be meshed using predefined mesh features. Also, when connecting two or more B splines without C^1 continuity, predefined mesh features are used. More details about these features can be found in Ref. 14.

The isoparametric element mapping function appears as

$$\boldsymbol{x}^T = \boldsymbol{N}\boldsymbol{X}^e, \qquad \boldsymbol{X}^e = \{\boldsymbol{x}_i^{eT}\}, \qquad i = 1, \ldots, 9 \tag{27}$$

with $\boldsymbol{x}_i^e$ from Eq. (24). The shape functions N for the nine node element are well established.[15]

Optimization Solution

In connection with beam cross-sectional shape optimization, several optimization problems can be posed. Here, only the behavior of a single structural member is included. Two classes of problems will be distinguished. The first is the application of cross-sectional properties as constraints and objective function. Then, the mass minimization appears as follows.

Objective:

$$A(\boldsymbol{p}) \Rightarrow \min \tag{28a}$$

Constraints:

$$I_{qr}^{l} \le I_{qr}(\boldsymbol{p}) \le I_{qr}^{u} \tag{28b}$$

$$a_{qr}^{l} \le a_{qr}(\boldsymbol{p}) \le a_{qr}^{u} \tag{28c}$$

where A is the cross-sectional area, and $I_{qr}, q, r = y, z; a_{qr}, q, r = x, y, z$ are the cross-sectional properties defined earlier. The maximization of the torsional constant I_t and other stiffness parameters with a prescribed cross-sectional area A belongs to the same class of problems. The second class of optimization problems that can be solved efficiently using this methodology is mass minimization under stress constraints. These problems can be expressed as follows.

Objective:

$$A(\boldsymbol{p}) \Rightarrow \min \tag{29a}$$

Constraints:

$$\left(\frac{\tau_{t\max}(\boldsymbol{p})}{\tau^{u}} - 1\right) \le 0 \tag{29b}$$

where $\tau_{t\max}$ is the maximum tangential shear stress on the boundary of the cross section. Additionally, side and equality constraints may apply.

Based on the mapping technique described earlier, the parameterization for shape optimization is quite simple. Techniques for altering rational B-spline curves can be used directly for changing the shape of the cross section to obtain an optimal solution. Design variables $p_j \in \boldsymbol{p}$ of the optimization problem are the coordinates $p_{j\beta} \in \boldsymbol{p}_j$ and weights w_j of the vertices of the defining polygons of the NURB curves. The convex hull property of rational B-spline curves leads to a simple formulation for physical constraints on the shape of the structure that has to be optimized, i.e., each constraint applied to the vertex coordinates also applies to the structural geometry.

An efficient way to obtain the solution of shape optimization problems is to use approximation methods. These methods use sequential solutions of approximate optimization problems to obtain the solution of the general structural optimization problem of Eq. (1). In the literature a wide variety of such methods can be found.[16] The optimization problem will be solved using convex linearization and a dual optimization method.[17–19] The iteration will be stopped if the relative change in the objective function is less than a given ϵ_w and the constraints are fulfilled within a vicinity of ϵ_g.

To reduce the numerical effort of the optimization process, equality constraints will be eliminated. These constraints will be linearized and then resolved. The design variables are separated into free and dependent variables $\boldsymbol{p}_f$ and $\boldsymbol{p}_d$, respectively.[20] Then, the equality constraints in Eq. (1) appear as

$$[\boldsymbol{H}_d \quad \boldsymbol{H}_f] \begin{bmatrix} \boldsymbol{p}_d \\ \boldsymbol{p}_f \end{bmatrix} = \boldsymbol{h} \tag{30}$$

Resolution leads to

$$\boldsymbol{p}_f = \boldsymbol{H}_f^{-1}[\boldsymbol{h} - \boldsymbol{H}_d \boldsymbol{p}_d] \tag{31}$$

The matrix $\boldsymbol{H}_f$ is invertible if the equality constraints are consistent. To introduce the equality constraints into the approximate optimization problem, the partial derivatives of the objective and the constraints have to be replaced by the total derivatives with respect to the free design variables, which for the constraint g_i are given by

$$\frac{\mathrm{d}g_i}{\mathrm{d}p_f} = \frac{\partial g_i}{\partial p_f} - \boldsymbol{H}_f^{-1}\boldsymbol{H}_d \nabla_d g_i \tag{32}$$

Sensitivity Analysis

For the formulation of the approximate optimization problem, the derivatives of the objective and constraints with respect to the design variables have to be calculated. Since the stresses and cross-sectional properties are given explicitly using the results of the finite element solution, the design sensitivities will be obtained analytically. Design variables are the vertex coordinates $\boldsymbol{p}_j$ and weights w_j of the NURB curves that define the shape of the cross section and the wall thickness.

Derivatives $\partial/\partial p_j$ with respect to the design parameter p_j will be marked by the subscript, j. To distinguish them from other derivatives, they will be called design derivatives.

Finite Element Equation

Express the derivatives of the element equation of Eq. (12) as

$$\boldsymbol{K}^e \boldsymbol{d}_{q,j}^e = \boldsymbol{f}_{q,j}^e - \boldsymbol{K}_{,j}^e \boldsymbol{d}_q^e \tag{33}$$

where the derivatives of the element matrix $\boldsymbol{K}^e$ can be obtained from

$$\boldsymbol{K}_{,j}^e = -\int_{-1}^{+1}\int_{-1}^{+1} \boldsymbol{B}^T \boldsymbol{A}_1 \boldsymbol{B} \det \boldsymbol{J}\, \mathrm{d}\xi\, \mathrm{d}\eta \tag{34}$$

with the abbreviation

$$\boldsymbol{A}_1 = \left[\boldsymbol{J}^{-1}\boldsymbol{J}_{,j}\right]^T - \boldsymbol{I}\frac{[\det \boldsymbol{J}]_{,j}}{\det \boldsymbol{J}} + \boldsymbol{J}^{-1}\boldsymbol{J}_{,j} \tag{35}$$

and the derivatives of the element vector $\boldsymbol{f}_q^e$ are

$$\begin{aligned} \boldsymbol{f}_{q,j}^e &= \boldsymbol{f}_{q1,j}^e + \boldsymbol{f}_{q2,j}^e \\ &= -\int_{-1}^{+1}\int_{-1}^{+1} \left[\boldsymbol{B}^T \boldsymbol{a}_1 - \boldsymbol{N}^T \nabla^T \boldsymbol{a}_2\right] \det \boldsymbol{J}\, \mathrm{d}\xi\, \mathrm{d}\eta \end{aligned} \tag{36}$$

with

$$\begin{aligned} \boldsymbol{a}_1 &= \left[\boldsymbol{J}^{-1}\boldsymbol{J}_{,j}\right]^T \boldsymbol{g}_q - \boldsymbol{a}_2, \\ \boldsymbol{a}_2 &= \boldsymbol{I}\frac{[\det \boldsymbol{J}]_{,j}}{\det \boldsymbol{J}} \boldsymbol{g}_q + \boldsymbol{g}_{q,j} \end{aligned} \tag{37}$$

Both Eqs. (34) and (36) can be further simplified. From the definition of the matrix $\boldsymbol{B}$ and the mapping function of Eq. (27), a matrix

$$\boldsymbol{A}_2 = \boldsymbol{J}^{-1}\boldsymbol{J}_{,j} = \boldsymbol{B}\boldsymbol{X}_{,j}^e \tag{38}$$

can be established, where $\boldsymbol{X}_{,j}^e$ is the design derivative of the element nodal coordinates of Eq. (44). The matrix $\boldsymbol{X}_{,j}^e$ is also called the design velocity field. Since two-dimensional elements are used, a simpler expression for $[\det \boldsymbol{J}]_{,j}$ can be found from Eq. (38). Then,

$$\frac{[\det \boldsymbol{J}]_{,j}}{\det \boldsymbol{J}} = A_{11} + A_{22} \tag{39}$$

where A_{11}, A_{22} are the main diagonal coefficients of the matrix $\boldsymbol{A}_2$ of Eq. (38).

Introduction of nodal compatibility of the design derivatives $\boldsymbol{d}_{q,j}$ leads to the system equation

$$\boldsymbol{K}\boldsymbol{d}_{q,j} = \boldsymbol{f}_{q,j} - \boldsymbol{K}_{,j}\boldsymbol{d}_q \tag{40}$$

If Cholesky's method is used to solve Eq. (15), the matrix $\boldsymbol{K}$ does not have to be factored again. Finally, the design derivatives of the gradient of ψ_q are obtained from

$$\nabla\psi_{q,j} = \boldsymbol{B}\left[\boldsymbol{d}_{q,j}^e - \boldsymbol{X}_{,j}^e \boldsymbol{B}\boldsymbol{d}_q^e\right], \qquad q = x, y, z \tag{41}$$

Design Velocity Field

To complete the design sensitivity analysis for the finite element equations, the design velocity field $\boldsymbol{X}^e_{,j}$ remains to be determined. This can be found by differentiating the nodal coordinates given by Eq. (24).

First, the derivatives with respect to the vertex coordinates and weights of the defining NURB curves will be given. For the element $\zeta_\gamma, \zeta_n, \zeta_\gamma \in \langle 1, \mu_\gamma \rangle, \zeta_n \in \langle 1, \mu_n \rangle$ they are found as

$$\boldsymbol{x}^e_{3(k-1)+l,j} = \boldsymbol{r}_{,j}(\gamma_k) + \boldsymbol{n}_{,j}(\gamma_k) \times \frac{2\zeta_n - \mu_n + l - 3}{2\mu_n} t - \boldsymbol{c}_{,j}, \qquad k, l = 1, 2, 3 \tag{42}$$

using γ_k of Eq. (25).

The design derivatives of the position vector $\boldsymbol{r}$ and its derivatives $\boldsymbol{r}^{(n)}$ with respect to the vertex coordinates $\boldsymbol{p}_j$ and weights w_j are found by differentiating Eqs. (19) and (21), respectively.[8,13] Then, also the design derivative $\boldsymbol{n}_{,j}$ of the normal vector on the curve can be determined.

If the wall thickness t is the design variable, the design derivatives of the nodal coordinates of the element $\zeta_\gamma, \zeta_n, \zeta_\gamma \in \langle 1, \mu_\gamma \rangle, \zeta_n \in \langle 1, \mu_n \rangle$ appear as

$$\boldsymbol{x}^e_{3(k-1)+l,t} = \boldsymbol{n}(\gamma_k) \frac{2\zeta_n - \mu_n + l - 3}{2\mu_n} - \boldsymbol{c}_{,t}, \qquad k, l = 1, 2, 3 \tag{43}$$

Note that a change of the wall thickness can force a change of the vertices of the defining NURB curves as, for example, for the beam of Fig. 1 at the welded parts. These dependencies can be introduced through equality constraints. With the derivatives of Eqs. (42) and (43), the design velocity field follows from

$$\boldsymbol{X}^e_{,j} = \left\{ \boldsymbol{x}^{eT}_{i,j} \right\}, \qquad i = 1, \ldots, 9 \tag{44}$$

For predefined mesh features used for areas with high curvature or for connections of B-spline curves, the design velocity field is computed analytically from the definition of the features.[14]

Cross-Sectional Properties and Stresses

The derivatives of the coefficients $a_{qr}, q, r = x, y, z$, and the shear center $s_q, q = y, z$, are efficiently obtained using the adjoint variable method.[21] These coefficients result from the sum of scalars of Eq. (17). For the quantities a_{qr1} and a_{qr2} of Eq. (18), an adjoint equation can be found. The adjoint equation for scalar a_{qr1} is the same as the finite element equation of Eq. (15), i.e., the adjoint variables are the solution of the finite element equation. For the scalar a_{qr2} the adjoint equation is

$$\boldsymbol{K}\boldsymbol{v}_q = \boldsymbol{f}_{q1} \tag{45}$$

which can be solved simultaneously with Eq. (15). The right-hand-side vector $\boldsymbol{f}_{q1}$ follows from the vector $\boldsymbol{f}_q$ of Eq. (14). From this, it can be seen that

$$a_{qr1,j} = \boldsymbol{d}_q^T [2 f_{r,j} - \boldsymbol{K}_{,j} \boldsymbol{d}_r] \tag{46}$$

and

$$a_{qr2,j} = \boldsymbol{d}_q^T \boldsymbol{f}_{r1,j} + \boldsymbol{v}_q^T [\boldsymbol{f}_{r1,j} - \boldsymbol{K}_{,j} \boldsymbol{d}_r] \tag{47}$$

Notice, that in case $\boldsymbol{f}_q = \boldsymbol{f}_x$, Eq. (45) is the same as Eq. (15). Hence, $\boldsymbol{v}_x = \boldsymbol{d}_x$. The numerical effort can be further reduced, if Eqs. (46) and (47) are calculated at the element level. Then,

$$a_{qr,j} = \sum_e \left\{ a^e_{qr1,j} - a^e_{qr2,j} - a^e_{rq2,j} + a^e_{qr3,j} \right\} \tag{48}$$

The derivatives of the area integrals, like $a_{qr3,j}, q, r = x, y, z$, $I_{qr,j}, q, r = y, z$ are obtained from

$$\frac{\partial}{\partial p_j} \int_A F(y, z)\, \mathrm{d}A = \sum_e \int_{-1}^{+1} \int_{-1}^{+1} \left[F(\xi, \eta)_{,j} + F(\xi, \eta) \frac{[\det \boldsymbol{J}]_{,j}}{\det \boldsymbol{J}} \right] \det \boldsymbol{J}\, \mathrm{d}\xi\, \mathrm{d}\eta \tag{49}$$

The design derivatives of the stresses have to be calculated by direct differentiation.[21] These derivatives are given by

$$\tau_{,j} = (\nabla \psi_{x,j} - \boldsymbol{g}_{q,j}) \phi'_x + (\nabla \psi_x - \boldsymbol{g}_q) \phi'_{x,j} + (\nabla \psi_{y,j} - \boldsymbol{g}_{q,j}) V_y + (\nabla \psi_{z,j} - \boldsymbol{g}_{q,j}) V_z \tag{50}$$

To obtain $\nabla \psi_{q,j}, q = y, z$, the system of Eqs. (40) has to be solved.

Numerical Example

A beam structure similar to Fig. 1 will be solved to demonstrate the technique described here. A similar example was used in Ref. 13. The sample beam is made of two welded parts. The NURB curves that define the cross-sectional shape and their defining polygons are shown in Fig. 5. The upper part of the shape is defined by a sixth-order NURB curve with two second-order curves on the ends, and the lower part is defined by a seventh-order NURB curve also with two second-order curves on the ends. The walls are modeled using three elements through the thickness. Along the NURB curves, the second-order curves were discretized by 6 elements each and the higher order curves by 50 elements each. Both parts are welded at the straight ends. Welding points are the nodes of the elements. The initial wall thickness is constant, $t = 2.0$. All weights w_i of the NURB curves were initially given as $w_i = 1$. The vertical side constraints are given by the broken lines in Fig. 5. An additional side constraint was imposed to prevent the structure from touching the point (50,100).

Four different sets of design variables that were selected are summarized in Table 1. The numbers of the vertex coordinates and weights refer to Fig. 5. The quantity t_u is the wall thickness of the upper part of the beam. Note that if t_u is employed, the vertices which define the welded ends of the upper part have to be used as additional design variables.

The optimal solutions were obtained using convex linearization with a dual optimization method. Specifics of the algorithm were given in Ref. 22. The solution cycle was interrupted after $s_{\max}$ iterations if the change in the objective function was less than 0.1% and the constraints were fulfilled within the same margin.

Three cross-sectional shape optimization problems are posed. First, the cross-sectional area is the two be minimized with constraints on the moments of inertia and torsional constants. The problem is given by

$$\begin{aligned} A &\Rightarrow \min \\ I_{yy} &\geq 0.120\ 10^7 \text{ units} \\ I_{zz} &\geq 0.035\ 10^7 \text{ units} \\ I_t &\geq 0.120\ 10^7 \text{ units} \end{aligned} \tag{51}$$

Table 1 Sets of design variables (DV)

Variant	Design variables	Free DV	Total DV
A	$p_{jy}, j = 1, 2, p_{jz}, w_j, j = 1, \ldots, 5, t_u$	13	21
B	$p_{jy}, j = 1, 2, p_{jz}, j = 1, \ldots, 5, t_u$	8	16
C	$p_{jy}, j = 1, 2, p_{jz}, w_j, j = 1, \ldots, 5$	12	12
D	$p_{jy}, j = 1, 2, p_{jz}, j = 1, \ldots, 5$	7	7

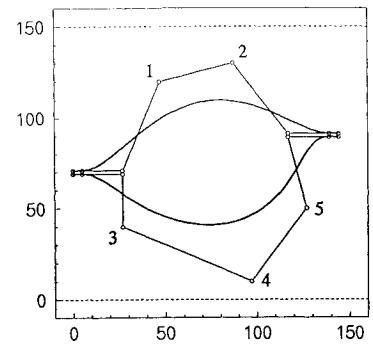

Fig. 5 Example, NURB curves and defining polygons of the initial design.

Table 2 Results of the problem of Eq. (51)

	Initial	A	B	C	D
A	660.1	596.1	665.6	697.1	711.7
I_t [10^7]	0.0794	0.1200	0.1200	0.1200	0.1200
I_{yy} [10^7]	0.1182	0.1200	0.1200	0.1288	0.1273
I_{zz} [10^7]	0.0328	0.0599	0.0625	0.0538	0.0603
s_{max}		9	7	5	4

Table 3 Results of the problem of Eq. (52)

	Initial	A	B	C	D
I_t [10^7]	0.0794	0.1883	0.1279	0.1234	0.1108
A	660.1	700.0	700.0	700.0	700.0
s_{max}		12	8	8	6

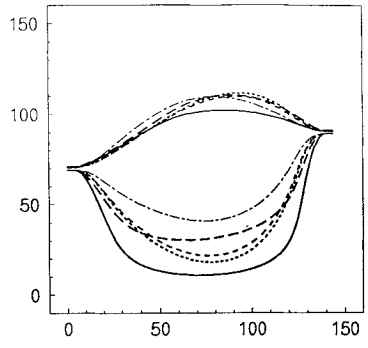

Fig. 6 Example, results of the problem of Eq. (51); optimal shapes, centerline of the NURB curves: —·—·—, initial; ——, A; - - - - -, B; — —, C; – –, D.

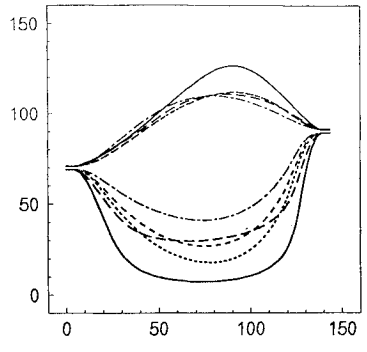

Fig. 7 Example, results of the problem of Eq. (52); optimal shapes, centerline of the NURB curves: —·—·—, initial; ——, A; - - - - -, B; — —, C; – –, D.

Figure 6 shows the shapes of the final and initial designs. The properties of the optimal solutions of this problem are given in Table 2. Second, the torsional constant is to be maximized under a prescribed cross-sectional area of 700.0 units. Hence, the problem reads

$$I_t \Rightarrow \max$$
$$A = 700.0 \text{ units} \tag{52}$$

The results are summarized in Fig. 7 and Table 3. Third, the cross-sectional area is to be minimized with a constraint on the maximum tangential shear stress. The beam is loaded with a torsional moment $M_x = 100$ units. The optimization problem appears as

$$A \Rightarrow \min$$
$$T_t\max \leq 0.5\ 10^{-2} \text{ units} \tag{53}$$

No feasible design configuration could be found for sets B and D of design variables. Figure 8 and Table 4 summarize the results.

Table 4 Results of the problem of Eq. (53)

	Initial	A	C
A	660.1	715.7	749.6
$\tau_{t\,max}$ [10^{-2}]	0.8523	0.5000	0.5000
I_t [10^7]	0.0794	0.1911	0.1714
s_{max}		11	5

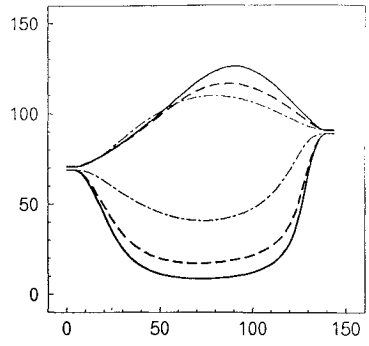

Fig. 8 Example, results of the problem of Eq. (53); optimal shapes, centerline of the NURB curves: —·—·—, initial; ——, A; — —, C.

Concluding Remarks

A geometry-based approach for the optimal shape design of thin-walled beam cross sections was presented. The geometric description of the cross-sectional shape with NURB curves was directly applied to the geometric definition of the finite element model. Parameterization of the structural shape was realized using the control of NURB curves. The thickness of the wall was included as a design variable. The direct application of NURB curves, which are important elements in CAD, for the description of the computational model makes the methodology attractive for coupling finite element analysis and optimization with CAD. Since the original structural geometry was modified during the optimization process, the results of the optimization can be transferred back into the CAD system easily. The use of rational B splines provides the opportunity to include vertex weights into the design space. The variety of functions that are available for the description of the design is extended into the space of rational functions. If simple B splines are used, the design space is a polynomial space. Using NURB curves a greater variety of design variables in available for shape optimization. That was demonstrated by the numerical example. Because of the expansion of the design space, the inclusion of rational functions for the shape definition led to further design improvements.

The methodology included three types of design variables for the optimization of thin-walled beam cross sections, vertex coordinates, vertex weights, and the wall thickness. The particular choice by the designer as to which design variable to include must be made according to the needs of the design and the availability of such control parameters in the tools actually used for the design. This paper provides methodology for improving the design of thin-walled beam structures which can be used in many applications.

Acknowledgment

The first two authors gratefully acknowledge the financial support of this project by Ford Motor Co., Dearborn, Michigan.

References

[1]DeVries, R. I., Saha, N. K., Suruli, P., and Zebrowski, M. P., "Structural Optimization of Beam Sections for Minimum Weight Subject to Internal and Crush Strength Constraints,"*Proceedings of the 6th International Conference on Vehicle Structural Mechanics*, SAE P-178, Society of Automotive Engineers, Warrendale, PA, 1986, pp. 47–51.

[2]Farin, G., *Curves and Surfaces for Computer Aided Geometric Design, A Practical Guide*, 2nd ed., Academic, San Diego, 1990, pp. 231–248.

[3]Anon., *Free-Form Geometry Representation (NURBS)*, Automotive Industry Action Group, AIAG-Pub. D-3 01.00 2/91, Southfield, MI, 1991.

[4]Braibant, V., and Fleury, C., "Shape Optimal Design using B-Splines," *Computer Methods in Applied Mechanics and Engineering*, Vol. 44, No. 3, 1984, pp. 247–267.

[5]Shyy, Y. K., Fleury, C., and Izadpanah, K., "Shape Optimal Design using High-Order Elements." *Computer Methods in Applied Mechanics and Engineering*, Vol. 71, No. 1, 1988, pp. 99–116.

[6]Chang, K.-H., and Choi, K. K., "A Geometry-Based Parameterization Method for Shape Design of Elastic Solids," *Mechanics of Structures and Machines*, Vol. 20, No. 2, 1992, pp. 215–252.

[7]Beltzinger, K.-U., and Ramm, E., "Structural Optimization as Tool for Shape Design," *Numerical Methods in Engineering'92, Proceedings of the First European Conf. on Numerical Methods in Engineering*, edited by C. Hirsch, O. C. Zienkiewicz, and E. Onate, Brussels, Belgium, 1992, pp. 465–478.

[8]Schramm, U., and Pilkey, W. D., "The Coupling of Geometric Descriptions and Finite Elements Using NURBs—A Study in Shape Optimization," *Finite Elements in Analysis and Design*, Vol. 15, No. 1, 1993, pp. 11–34.

[9]Love, A. E., *A Treatise on the Mathematical Theory of Elasticity*, 4th ed., Dover, New York, 1994, pp. 329–335.

[10]Schramm, U., Kitis, L., Kang, W., and Pilkey, W. D., "On the Shear Deformation Coefficient in Beam Theory," *Finite Elements in Analysis and Design*, Vol. 16, No. 2, 1994, pp. 141–162.

[11]Rogers, D. F., and Adams, J. A., *Mathematical Elements for Computer Graphics*, McGraw–Hill, New York, 1976.

[12]Surana, K. S., "Isoparametric Elements for Cross-Sectional Properties and Stress Analysis," *International Journal for Numerical Methods in Engineering*, Vol. 14, No. 4, 1979, pp. 475–497.

[13]Schramm, U., and Pilkey, W. D., "Optimal Shape Design for Thin-Walled Beam Cross Sections Using NURB Curves," *International Journal for Numerical Methods in Engineering*, Vol. 37, No. 23, 1994, pp. 4039–4058.

[14]Kittleson, A. P., "Optimal Shape and Spot Weld Design for Thin-Walled Beam Cross Sections," M.S. Thesis, Univ. of Virginia, Dept. of Mechanical, Aerospace, and Nuclear Engineering, Charlottesville, VA, Jan. 1995.

[15]Bathe, K.-J., *Finite Element Procedures in Engineering Analysis*, Prentice–Hall, Englewood Cliffs, NJ, 1982, p. 200.

[16]Morris, A. J., *Foundations of Structural Optimization: A Unified Approach*, Wiley, New York, 1982.

[17]Starnes, J. H., and Haftka, R. T., "Preliminary Design of Composite Wings for Buckling, Strength and Displacement Constraints," *Journal of Aircraft*, Vol. 16, No. 8, 1979, pp. 564–570.

[18]Fleury, C., "Structural Weight Optimization by Dual Methods of Convex Programming," *International Journal for Numerical Methods in Engineering*, Vol. 14, No. 12, 1979, pp. 1761–1783.

[19]Braibant, V., and Fleury, C., "An Approximation Concepts Approach to Shape Optimal Design," *Computer Methods in Applied Mechanics and Engineering*, Vol. 53, No. 2, 1985, pp. 119–148.

[20]Fleury, C., Zong, W.-H., and Duysinx, P., "An Integrated Design Approach to Structural Shape Optimization," *Proceedings of the Structural Optimization '93—The World Congress on Optimal Design of Structural Systems*, edited by J. Herskovits, Vol. 1, Associação Brasiliera de Ciências Mecânicas, Rio de Janeiro, Brazil, 1993, pp. 101–108.

[21]Haug, E. J., Choi, K. K., and Komkov, V., *Design Sensitivity Analysis of Structural Systems*, Academic, Orlando, FL, 1986, pp. 25–48.

[22]Schramm, U., and Pilkey, W. D., "Structural Shape Optimization for the Torsion Problem using Direct Integration and B-Splines," *Computer Methods in Applied Mechanics and Engineering*, Vol. 107, Nos. 1–2, 1993, pp. 251–268.